Heliyon 6 (2020) e04085

Contents lists available at ScienceDirect

Heliyon

journal homepage: www.cell.com/heliyon

Research article

Hydroxyapatite nanoparticles derived from mussel shells for *in vitro* cytotoxicity test and cell viability

Gehan T. El-Bassyouni [a], Samah S. Eldera [b,c], Sayed H. Kenawy [a,d], Esmat M.A. Hamzawy [e,*]

[a] Refractories, Ceramics and Building Materials Dept., National Research Centre, 33 El Buhooth St., Dokki, Cairo, 12622, Egypt
[b] King Abdulaziz University, Faculty of Science, Physics Dep., Jeddah, Saudi Arabia
[c] Physics Department, Faculty of Science Al-Azhar University, Cairo, Egypt
[d] Imam Mohamed Ibn Saud Islamic University (IMSIU), Collage of Science, Chemistry Dept. Riyadh, 11623, Saudi Arabia
[e] Glass Research Dept., National Research Centre, 33 El Buhooth St., Dokki, Cairo, 12622, Egypt

ARTICLE INFO

Keywords:
Biomedical engineering
Cluster of nanoparticles
Hydroxyapatite
Mussel shell
Stem cells
Tissue engineering

ABSTRACT

Hydroxyapatite (HA) nanoparticles derived from mussel shells were prepared using the wet precipitation method and were tested on human mesenchymal and epithelial cells. Shells and HA powder were characterized via X-ray diffraction analysis (XRD) and scanning electron microscopy along with energy dispersive X-ray spectroscopy (SEM/EDX), high resolution transmission electron microscopy (HR-TEM) and Fourier transform infrared spectroscopy (FTIR). The in vitro cytotoxic properties of HA and mussel shells were determined using sulphorhodamine B (SRB) assays for MCF-7 cells (HepG2) and colon (Caco-2) cells. Cell viability tests confirmed the nontoxic effects of synthesized HA and mussel shells on human mesenchymal stem cells (h-MSCs) and epithelial cells. Toxicity values were less than 50% of the cell's validity ratio based on analyses using different concentrations (from 0.01 to 1,000 μg). The results indicate that MSC and epithelial cell attachment and proliferation in the presence of both HA and shell occurred.

The proliferation capability was established after 3 and 7 days. SEM images revealed that stem cells and epithelial cells attached to the scaffold indicated full and complete integration between the cells and the material. It seems that due to the ion exchange between bovine serum albumin solutions (BSA) and HA, the FTIR data confirmed an increase in the amide I and amide II bands, which indicates the compatibility of the BSA helix structure. This study sheds light on the importance of merging stem cells and nanomaterials that may lead to improvements in tissue engineering to develop novel treatments for various diseases.

1. Introduction

In the medical field, the use of nanotechnology has advanced. The need for inventing new therapeutic biomaterials that can be employed as substrates for cell reproduction, bonding, multiplication and development has recently become essential [1]. For this purpose, hydroxyapatite (n-HA) nanoparticles were created using the wet chemical precipitation method from calcium-rich biowastes (mussel shells) [2, 3]. Hydroxyapatite is a biomineral with excellent biocompatibility and osteoconductivity, which makes it a commonly used material for drug delivery, orthopedic intervention, tissue engineering and dental implant applications [4, 5]. HA demonstrates good bioactivity and porosity and is an excellent candidate for bone repair and substitution. Similarly, due to its surface properties of ion exchange, low solubility and high water stability, HA has attracted attention as a vital absorbent for removing heavy metals from polluted water [6].

Tissue engineering consists of in vitro construction of tissues for implantation into the body to preserve or expand the forms and/or functions of particular tissues [7]. Presently, with the development of molecular biology and cell culture techniques, the growth behavior of cells seeded on materials has received attention. For cell cultures, human mesenchymal stem cells (h-MSCs) are commonly used when investigating cell viability for bone tissue engineering purposes [8].

Mesenchymal stem cells (MSCs) can differentiate along different genealogies such as bone lines (osteoblasts), cartilage (cartilage cells), fats (adipocytes), and muscles (muscle cells) [9]. Several studies have

* Corresponding author.
E-mail address: ehamzawy9@gmail.com (E.M.A. Hamzawy).

https://doi.org/10.1016/j.heliyon.2020.e04085
Received 11 September 2019; Received in revised form 5 March 2020; Accepted 22 May 2020

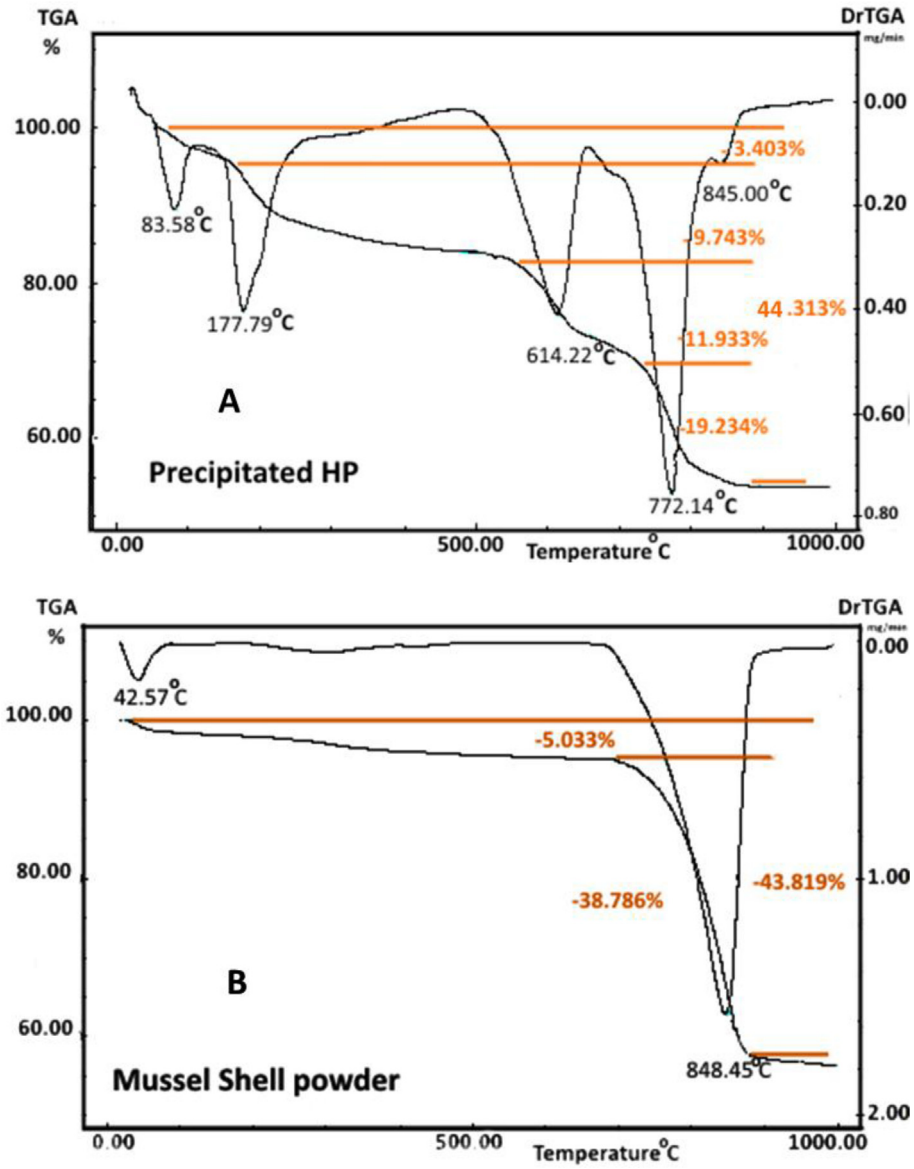

Figure 1. Thermogravimetric analysis of (A) HA sample and (B) mussel shell powder (after being dry at 70 °C for a few days).

investigated the influence of different materials on bone proliferation including biphasic calcium phosphate (BCP) ceramics [10, 11], hydroxyapatite [12], β-tri-calcium phosphate (β-TCP) [13], hydroxyapatite and mineralized collagen [14, 15].

In different biotechnological and medical applications, the protein adsorption method is the primary step after the contact of body fluids with solid surfaces. Protein adsorption of implant materials is of great importance for bond formation. This adsorption can proceed due to electrostatic and hydrophobic interactions between the protein and material surfaces [16].

Hydroxyapatite works as a hard tissue-implant material that enhances bone growth within the bone tissue. The bone implant interface includes a so-called retention zone, which consists of a protein matrix rich in calcium and phosphorous [17].

Based on the essential role of protein adsorption in tissue engineering, the present work deals with testing mussel shell and HA nanoparticle powder for their in vitro cytotoxic properties using sulforhodamine B (SRB) assays against MCF-7, liver (HepG2) and colon (Caco-2) cells.

2. Materials and methods

2.1. Hydroxyapatite synthesis

A variety of techniques for synthesizing hydroxyapatite have been established. In this study, we used the precipitation method to produce hydroxyapatite from mussel shells. This procedure is a low cost, simple process with high yield and is therefore appropriate for large-scale production.

In the present work, we created hydroxyapatite nanoparticles based on mussel shells, which have a high calcium carbonate content ($CaCO_3$) of nearly 98.62% [18]. The mussel shells were ultrasonically cleaned of organic matter using tap water before being dehydrated at room temperature. Washed, dehydrated shells were ground into fine particles using an agate ball mill. Calcium carbonate (29.36 g of powder) was transformed into a calcium nitrate $Ca(NO_3)_2$ solution using concentrated nitric acid (HNO_3) while stirring vigorously, and this resulted in the discharge of carbon dioxide (CO_2) gas.

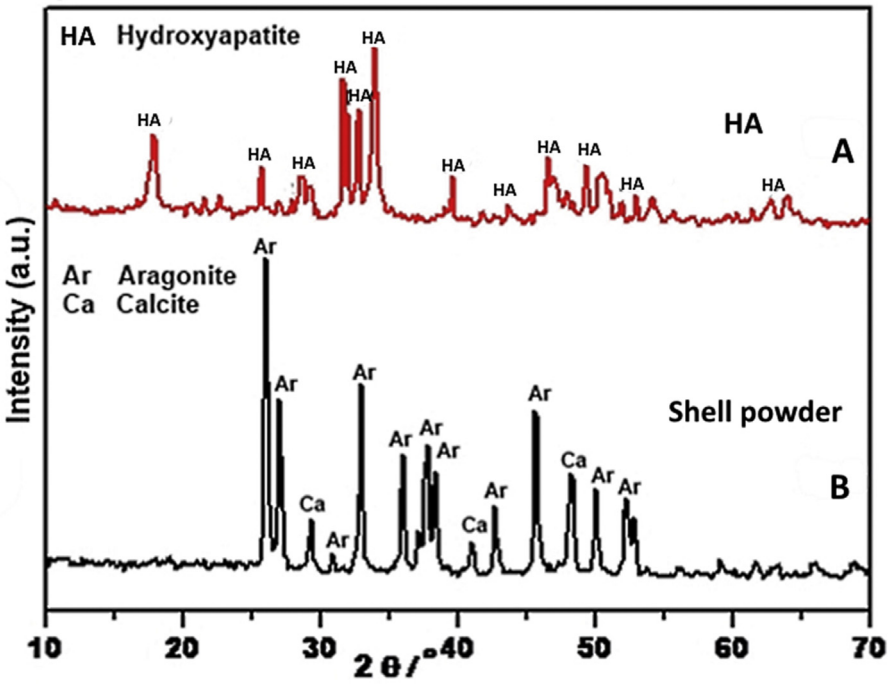

Figure 2. X-ray diffraction patterns of (A) HA and (B) mussel shell powder (calcined at 900°C/2 h).

A stoichiometric quantity of ammonium dihydrogen-phosphate ($NH_4H_2PO_4$) solution was gradually added to the $Ca(NO_3)_2$ solution while stirring [19]. The pH of the mixture reached 9 by the addition of 3 M 25% ammonium hydroxide (NH_4OH). Next, the mixture was stirred magnetically and the precipitate was then dehydrated at 70 °C for a few days and was then crushed in a mortar. Finally, the resultant HA powder was formed after calcination at 900 °C.

2.2. Characterization of materials

The chemical composition of the mussel shells was determined using X-ray fluorescence (XRF) with a modern wavelength dispersive spectrometer (Axios PAN analytical 2005, Netherlands). A thermogravimetric (TGA) analyzer (TGA-50, Shimadzu, Japan) was used to examine the synthetized HA and shells. The TGA curve increased from room temperature to 1,000 °C with a warming rate of 10 °C/min. The shells and synthesized HA powders (calcined at 900 °C) were analyzed by X-ray diffraction (XRD) using a D8 Advanced CuO target (Bruker, Germany)-based generator X-ray diffractometer using CuKα radiation (λ = 1.542 Å). X ray diffraction graphs were recorded in the range of 2θ = 10–70° at a scan speed of 2 °C/min. The fresh shell surfaces and synthesized HA were sputtered with a thin gold layer before being examined by scanning electron microscopy (SEM/EDX, model FEJ Quanta 250 Fei, Holland) and the material configurations were chemically analyzed via attached energy-dispersive X-ray spectroscopy (EDX). Likewise, for examining the HA particles, a dilute suspension of HA particles was prepared and dropped onto copper grids sustained with a carbon film. The HA particle shapes and sizes were determined by phase-contrast imaging using high-resolution transmission electron microscopy (HR-TEM, JEOL JXA-840 A, Electron probe microanalyzer, Japan). Infrared spectra were obtained with a Fourier transform infrared (FTIR) spectrophotometer (model FT/IR-6100 type A, USA). FTIR spectra were obtained in the range of 2,200-400 cm^{-1} using the KBr technique.

2.3. In vitro studies

2.3.1. Cell cultures

HA and mussel shell powders were subjected to cellular cytotoxicity evaluations on both normal and cancer cell lines. Doxorubicin (Dox), which is a commonly used chemotherapy medicine used to treat different cancers, was used as a positive control [20]. Dox is an influential iron-chelator that directly binds to DNA via intercalation between the base pairs on the DNA helix [21]. The excessive oxidative stress caused by Dox changes the diversity of cellular molecules [22]. Samples were dissolved in 20% dimethyl sulfoxide (DMSO). The DMSO was diluted so that its final concentration was 1 mg/mL to mitigate its cytotoxic effects at high concentrations [23].

Sulforhodamine B (SRB) assays were used to resolve the in vitro cytotoxic activities of the HA and mussel shells. A mammary gland breast cancer cell line (MCF-7), human hepatocellular carcinoma cell line (HepG-2), and colon carcinoma cell line (Caco-2) were all maintained at the Cell Culture Lab, Egyptian Organization for Biological Products and Vaccines (VACSERA Holding Company) Cairo, Egypt. SRB assays were based on the uptake of the negatively charged pink amino-xanthine dye [24]. Similarly, cytotoxic evaluations of HA and shells for two types of normal cells (e.g., h-MSC and epithelial cells) were carried out. These cell lines were obtained from the VACSERA-Cell Culture Unit, Cairo, Egypt. The reagents RPMI-1640 medium, SRB and DMSO were purchased from the Sigma Company St. Louis, USA. Fetal bovine serum was obtained from GIBCO, UK. The cells were cultured in RPMI-1640 medium with 10% v/v fetal bovine serum. Two types of antibiotics (e.g., penicillin 100 units/mL and streptomycin 100 mg/mL) were used throughout the experiment. The cells were grown in a moistened incubator with a CO_2 atmosphere (5% v/v) at 37 °C and were seeded at a density of 1.0×10^4 cells/well in a 96-well plate at 37 °C for 48 h in 5% CO2. After incubation, the cells were treated with different concentrations of compounds and were incubated for 3 and 7 days and then compared with untreated control cells. For each individual dose, triplicate wells were prepared. The medium was discarded and fixation was accomplished using 10% trichloroacetic acid (TCA) at 150 mL/well for 1 h at 4 °C. The cells were washed three times using distilled water (TCA reduced the SRB binding of protein). The wells were discolored using SRB 70 mL/well for 10 min at room temperature with 0.4% 70 mL/well (kept in a dim place). After staining, washing was accomplished using 1% glacial acetic acid to eliminate the unbound dye (until clear drainage was reached). The plates were air dehydrated for 24 h and the dye was solubilized with 50 mL/well of 10 mM tris base of pH 7.4 for 5 min on a shaker at 1,600 rpm. The optical density of each well was

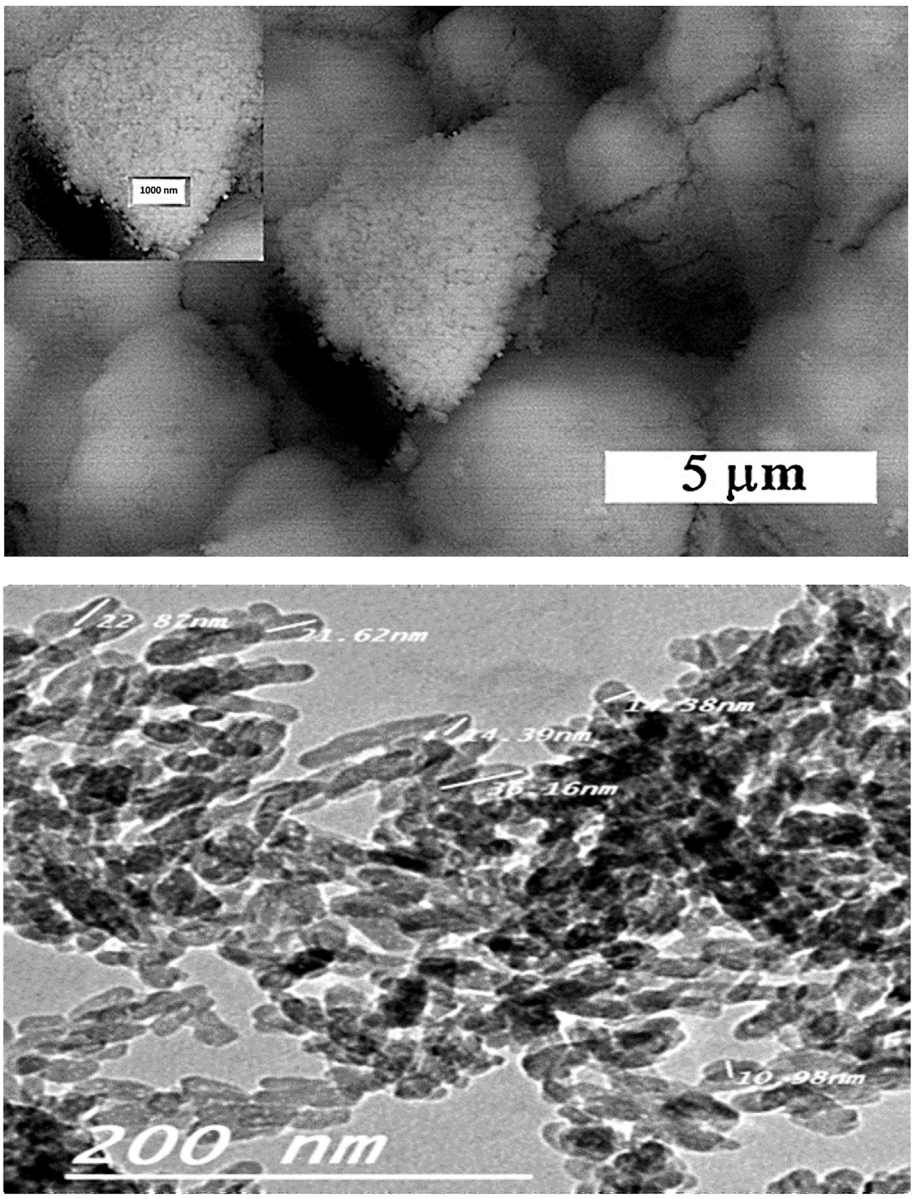

Figure 3. SEM and TEM images of HA sample sintered at 900°C/2 h.

determined at a wavelength 570 nm using an ELISA microplate reader (EXL800 USA)) Center of Genetic Engineering, Faculty of Science, Al-Azhar University, Cairo, Egypt). The relative cell viability percentage was calculated using the following formula:

[(A_{570} of treated sample/A_{570} of untreated sample) 100]

Sigma Plot software ver. 12.0 (Systat Software, Inc) was used for calculation of the IC50 values [25].

2.3.2. Protein adsorption

Protein adsorption levels on the tested surfaces were determined. Bovine serum albumin (BSA) was used as a representative protein. Approximately 0.2 mg of BSA was added to 200 ml of phosphate buffer solution (PBS) (dissolve 8 g of NaCl, 0.2 g of KCl, 1.805 g $Na_2HPO_4.2H_2O$ and 0.30717 g K_2HPO_4 in 800 ml distilled H_2O. Adjust pH to 7.4 using HCl. Complete volume to 1 L using distilled H_2O) at pH 7.4 and 37 °C. Four milligrams of each sample was added to 40 ml of the previous mixture. Adsorption was allowed to proceed in an incubator for 1 h at 37 °C. Upon adsorption, the samples were carefully rinsed with (PBS) 3 times and with water to remove unbound proteins (non-adsorbed) and salt residues and were then dried at 37 °C. Protein adsorption on the surface of the samples was determined by means of FTIR.

3. Results and discussion

3.1. Characterization of samples

The mineral composition of mussel shells was determined using the X-ray fluorescence (XRF) technique. It showed that the primary elements were Ca: 55.317% and C: 43.300% and the minor elements were Na: 0.465%, Si: 0.193% and Sr: 0.208%.

The results of thermogravimetric analysis (TGA) of HA and mussel shell powders are shown in Figure 1. The mussel shell samples exhibited early dehydration due to moisture followed by decarbonization at ~850 °C. The total weight loss was 43.819%. The prepared hydroxyapatite tracked the following steps:

Mussel shell powder ($CaCO_3$) + Nitric acid (HNO_3) → $Ca(NO_3)_2$ + CO_2 + H_2O

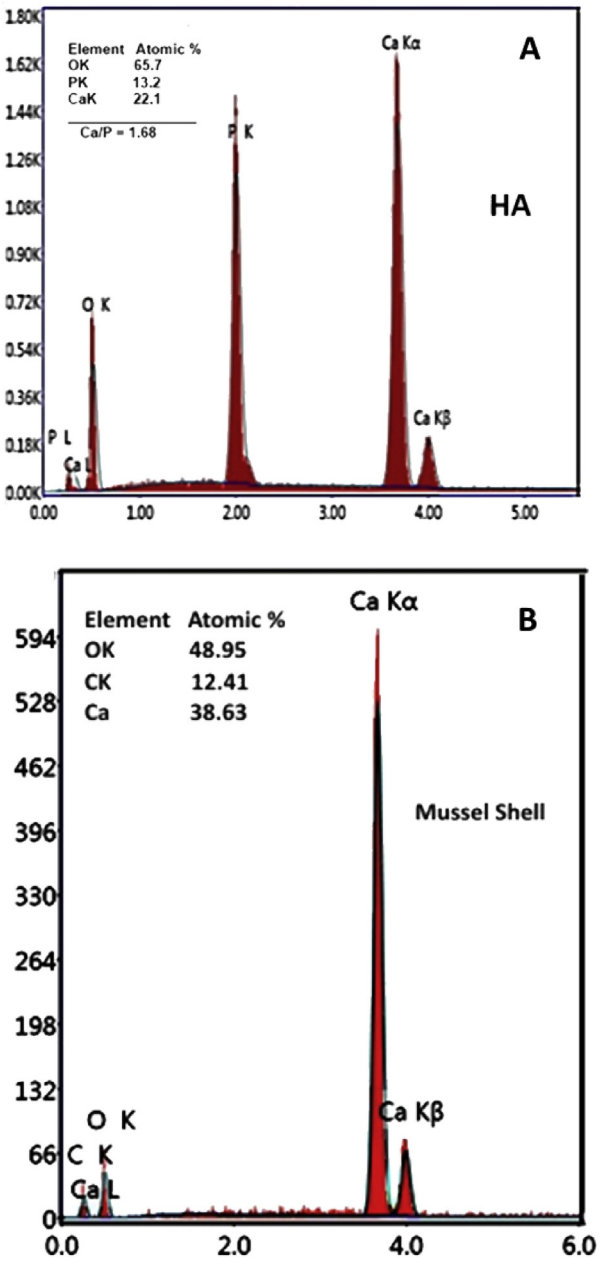

Figure 4. EDX microanalysis of (A) HA and (B) mussel shell powder (calcined at 900°C/2 h).

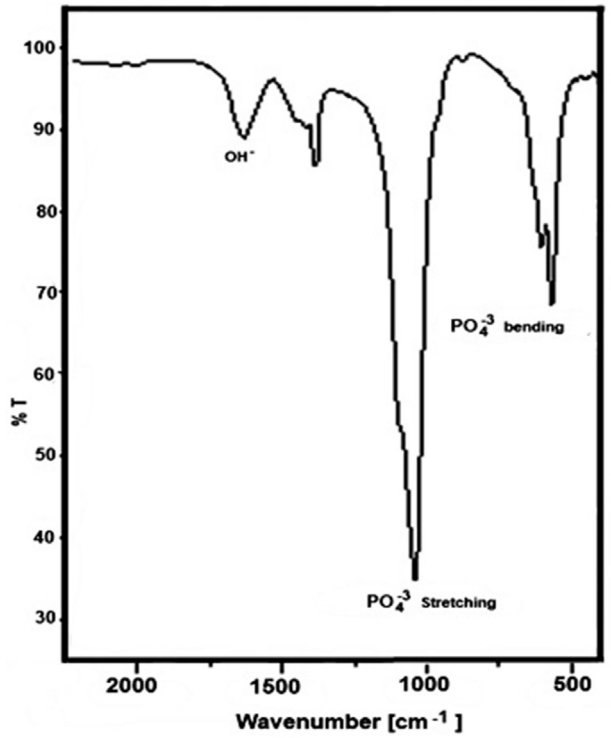

Figure 5. FTIR spectrum of the synthesized HA sample (calcined at 900°C/2 h).

$Ca(NO_3)_2$ + Ammonium dihydrogen phosphate ($NH_4H_2PO_4$) → Ca_2PO_4 + NH_4NO_3

Ca_2PO_4 + CaO (from solution) → Ca_{10} $(PO_4)_6(OH)_2$

Drying of the solution at 100 °C for a long duration (12 h) removed water; however, the precipitated hydroxyapatite [Ca_{10} $(PO_4)6(OH)_2$] was accompanied by the emission of CO_2, residual H_2O and ammonium nitrate (NH_4NO_3). TGA analysis of the HA sample showed dehydration (up to 177.79 °C) followed by decarbonation (-CO_2, between 700-900 °C) and denitration and dehydroxylation [-NH_4NO_3 up to 845 °C] (Figure 1) [26, 27]. The total weight loss was 44.313%.

The X-ray diffraction patterns of the shell powder demonstrated the presence of aragonite and a small amount of calcite as shown in Figure (2). X-ray analysis of the prepared HA (sintered at 900 °C) showed the formation of pure hydroxyapatite. Furthermore, in the HA diffractogram, sharp peaks and a straightforward baseline indicated that the synthetized HA was finely crystallized [3].

The SEM micrograph of HA, which was sintered at 900°C/2 h, displayed an agglomerate of ultrafine grain shapes of uniform size and solid structure. The HA clusters contained nanocrystals with diameters from 80 to 200 nm (Figure 3A). TEM micrographs revealed additional details of the nanohydroxyapatite clusters and clear nanoparticles between 10 and 40 nm (Figure 3B).

The results of EDX microanalysis of mussel shell and HA powders sintered at 900 °C are shown in Figure 4. EDX microanalysis of the mussel shell powder demonstrated that the constituent was $CaCO_3$ (i.e., Ca, C and O), which agrees with the XRF results. EDX for HA showed that the constituent was HA (i.e., Ca, P and O) and that the Ca/P atomic ratio was 1.68, which is almost identical to the stoichiometric ratio of 1.67 for pure HA. Ramesh et al., reported that the Ca/P ratio is a significant parameter that determines the properties of hydroxyapatite bioceramics [28]. For calcium-deficient HA, the Ca/P ratios are less than 1.67, while for calcium-rich HA, the Ca/P ratios are greater than 1.67.

All characteristic bands of HA were observed in the FTIR spectrum, as presented in Figure 5. The spectrum showed absorption bands at 1,000–1,100 (υ3-asymmetric stretching vibration) and 577–603 (υ4-asymmetric bending vibration), which were attributed to phosphate (PO_4^{3-}) absorption. The absorption band at 1,390 cm^{-1} resulted from the vibration of the CO_3^{2-} group and indicated the presence of carbonated hydroxyapatite (c-HA). The absorption band at 3,570 cm^{-1} was assigned to the stretching mode of hydrogen-bonded OH^- ions [29].

3.2. The in vitro cytotoxic activities of the HA and shells toward human cancer cells

SRB assays have been used to explore cytotoxicity in cell-based studies. The SRB assays evaluated the cytotoxicity of HA and shells for three cancer-cell lines *(e.g., MCF-7, HepG2 and Caco-2)* over a

Table 1. The IC_{50} (μg) of materials against different tumor and normal cell lines.

Materials	IC_{50} (μg)				
	MCF-7	HepG2	Caco-2	MSCs	EPI
HA	1548.3 ± 1.2	2520.7 ± 5.0	3520.6 ± 5.1	2981.6 ± 5.1	3250.0 ± 2.7
Shell	1343.7 ± 3.5	3859.0 ± 4.0	3829.0 ± 2.0	3543.0 ± 2.9	3670.0 ± 2.5

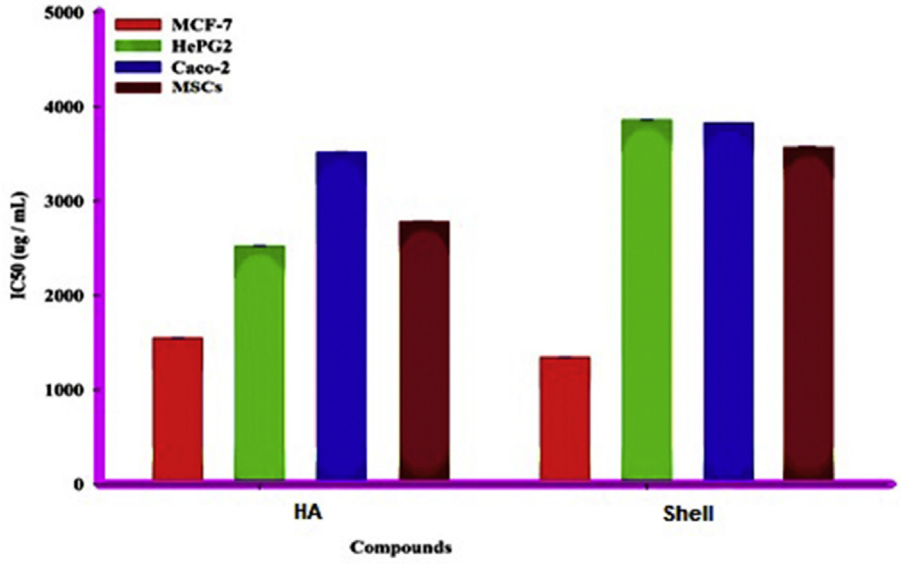

Figure 6. Bar chart representing the differences in IC_{50} for different tumor and normal cells (e.g., MCF-7, HePG2, Caco-2, MSCs and epithelial cells) after incubation with HA (calcined at 900°C/2 h) sample and mussel shells.

concentration range from 0.01 to 1,000 μg. HA and shell materials showed weaker cytotoxicity toward all solid tumor cells. The toxicities of HA and shell materials to MCF-7 cells were greater than for liver (HepG2) and colon (Caco-2) cells with IC50 values of 1,548.3 ± 1.2 and 1,343.7 ± 3.5 μg, respectively (Table 1 and Figure 6). Consequently, the HA and shells are nontoxic to human mesenchymal stem cells (h-MSCs) with IC50 values of 2,981.5 ± 3.9 and 3,543 ± 2.9 μg, respectively, and both materials are also nontoxic for epithelial cells with IC50 values of 3,250.0 ± 2.7 and 3,670.0 ± 2.5 μg, respectively, as shown in Table 1 and Figure 7.

Figure 6 shows the morphological observations of cells that were obtained after the samples were exposed to two types of normal human cells and three types of cancer cells. No dead cells were detected in the well plates containing the HA or shells, which confirmed that both samples had no negative effects in the natural cell environment. After 3 days of incubation, the growth of normal and cancer cells was estimated and the number of cells increased for seven days (Table 1). Cell viability assays revealed that IC50 (e.g., minimum concentration required to induce 50% of cell death after exposure to samples) could not be attained. For different concentrations of HA and shells, the toxicity values were less than 50% of the cells' validity ratio. These results may be attributed to the nontoxic properties of the tested materials (Figure 7).

Moreover, two types of normal cells (e.g., MSCs and epithelial), which were seeded on tissue cultures, showed significant differences in cell numbers after 3 and 7 days of incubation Figure (8A and B). The number of listed MSCs cells after 3 days of incubation of HA and mussel shells powders increased to 1.9×10^3 ± 2.3 and 1.86×10^3 ± 2.7, respectively, compared to the control, which exhibited 2.83×10^3 ± 1.9 cells. In contrast, the numbers of inserted epithelial cells after 3 days of incubation of HA nanoparticles and shells also increased to 2.7×10^3 ± 2.7 and 2.5×10^3 ± 3.0, respectively, compared to the control, which exhibited 3.82×10^3 ± 2.5 cells. The number of registered MSCs cells after 7 days of incubation of HA and shells increased to 2.82×10^3 ± 2.7 and 2.765×10^3 ± 1.8, respectively, compared to the control, which exhibited 2.98×10^3 ± 3.1 cells; the number of recorded epithelial cells after 7 days of incubation of samples HA and shells increased to 3.6×10^3 ± 2.9 and 3.4×10^3 ± 3.4, respectively, compared to the control, which exhibited 4.1×10^3 ± 2.6 cells (Table 2). These results suggest that attachment and proliferation of MSCs and epithelial cells in the presence of both HA and shell occurred.

The scanning electron microscopy (SEM) images show that the stem cells and epithelial cells require the HA and mussel shell, indicating complete association between the cells and tested materials (Figure 9).

Interestingly, the improvement of stem cell biology and nanotechnology has enhanced the opportunities for tissue engineering by increasing the attachment, proliferation and differentiation of stem cells in vitro. Accordingly, the modified nanomaterials require further in vivo studies to aid in the improvements of organ transplantation [30].

HA samples can be a profoundly osteoconductive biomaterial of clinical importance. HA stimulates the expansion of bone arrangement on the embedded surface, and newly synthesized bone is found in coordinated contact with the HA layer [31, 32, 33, 34].

MSCs can differentiate into osteoblasts, and they can differentiate to a variety of other cells such as chondrocytes, osteoblasts and adipocytes [35]. The aim of the present study was to determine whether clusters of HA nanoparticles and mussel shell would improve adhesion of MSCs and epithelial over the two different time periods (e.g., 3 and 7 days) and to compare the results to the two immersion periods.

It was found that MSCs and epithelial cells bound more to HA and mussel shell during an immersion time of 7 days when compared with a 3 day immersion time, and these results agree with those of other investigators. However, we observed that HA and mussel shells are not sufficient to promote full cell spreading, as is shown in Figure (8). Growth of mesenchymal stem cells and epithelial cells also appeared naturally without the addition of any external growth factors (GF).

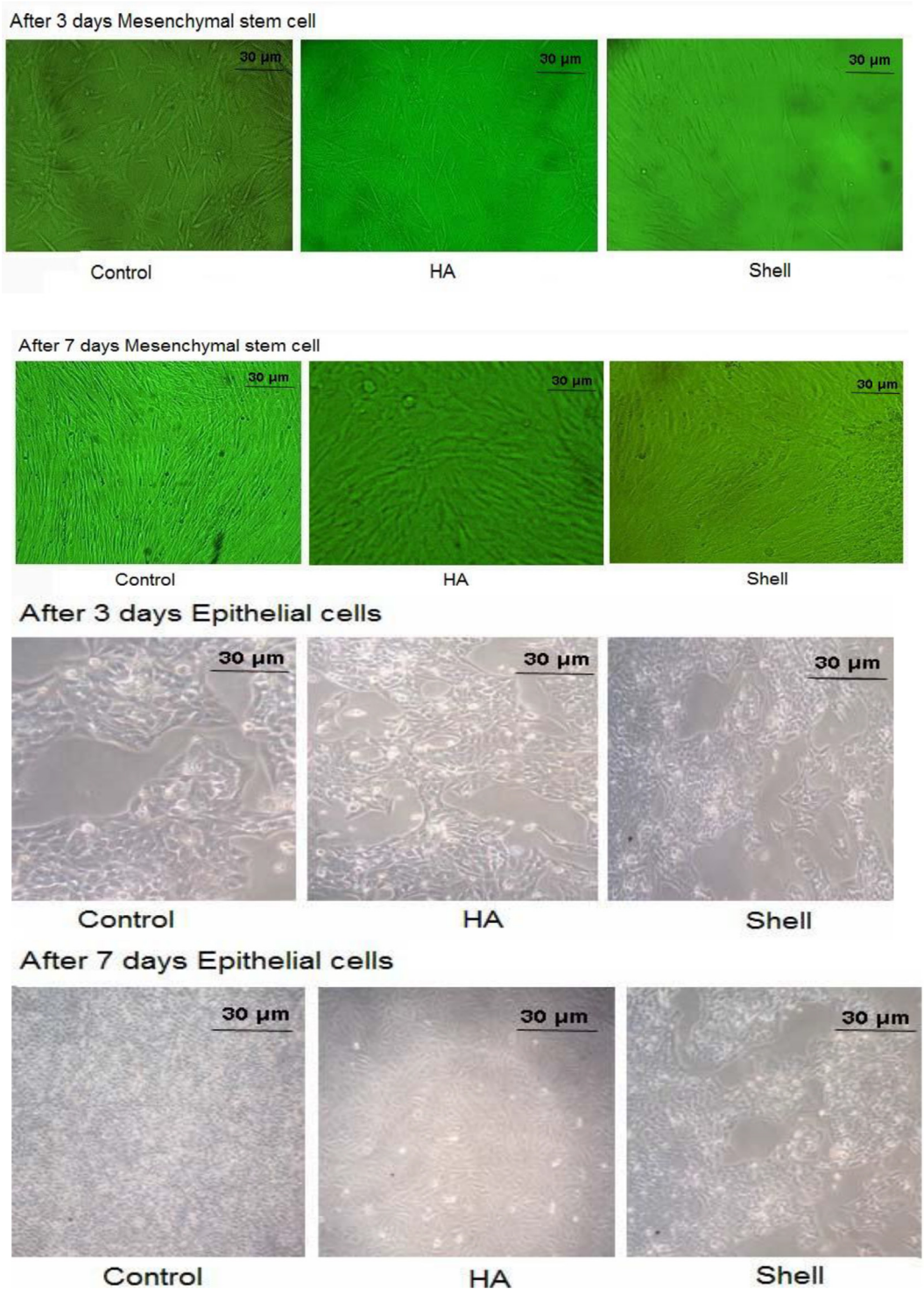

Figure 7. Light microscopy micrographs for normal cells (e.g., MSCs and epithelial cells) in cell cultures which show the nontoxicity of HA sample and shells.

3.3. Protein adsorption

3.3.1. FT-IR analysis of adsorbed BSA

FT-IR is sensitive to secondary protein structures. Proteins can bond with HA by electrostatic forces between the calcium ions and carboxyl groups and phosphate ions and amino groups [36]. The Amide I band is related to the C=O stretching of the peptide bonds [37].

The process of protein adsorption onto HA began with the formation of an anion layer such as $H_2PO_4^{-3}$ and OH^- on the HA surface, which was followed by a dispersive double electrical layer around the surface [38].

At that point, protein atoms were adsorbed through specific electrostatic interactions between charged groups of proteins and Ca^{2+} and hydrogen holding (irregular interactions), which may occur between neighboring protein atoms with polar surfaces [39]. For acidic proteins such as BSA, the carboxyl group is adsorbed to Ca^{2+} through the displacement of PO_4^{-3}. At the HA surface, the modification of BSA would be changed by NH_3, which may form hydrogen bonds with the phosphate group in HA [40].

The adsorption action of BSA on HA nanoparticles is mainly due to electrostatic interactions between the Ca^{2+} cations and $PO^{-3}{}_4$ anions of

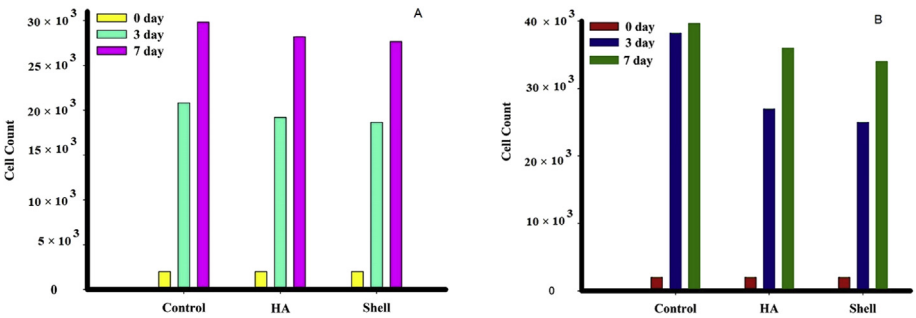

Figure 8. Bar chart representing: A. Cell proliferation assays showing the cell counting of MSCs and B. Epithelial cells after treatment with shells and HA-NPs for 3 and 7 days.

Table 2. The cell counting of MSCs an Epithelial cell after treatment with materials for 3 and 7 days.

	MSCs			Epithelial cells		
	0 Day cell/mL	3 days cell/mL	7 days cell/mL	0 Day cell/mL	3 days cell/mL	7 days cell/mL
Control	$2.0 \times 10^3 \pm 3.5$	$2.83 \times 10^3 \pm 1.9$	$2.98 \times 10^3 \pm 3.1$	$2.0 \times 10^3 \pm 3.5$	$3.82 \times 10^3 \pm 2.5$	$4.1 \times 10^3 \pm 2.6$
HA	$2.0 \times 10^3 \pm 2.8$	$1.9 \times 10^3 \pm 2.3$	$2.82 \times 10^3 \pm 2.7$	$2.0 \times 10^3 \pm 2.8$	$2.7 \times 10^3 \pm 2.7$	$3.6 \times 10^3 \pm 2.9$
Shell	$2.0 \times 10^3 \pm 2.4$	$1.865 \times 10^3 \pm 2.7$	$2.765 \times 10^3 \pm 1.8$	$2.0 \times 10^3 \pm 2.4$	$2.5 \times 10^3 \pm 3.0$	$3.4 \times 10^3 \pm 3.4$

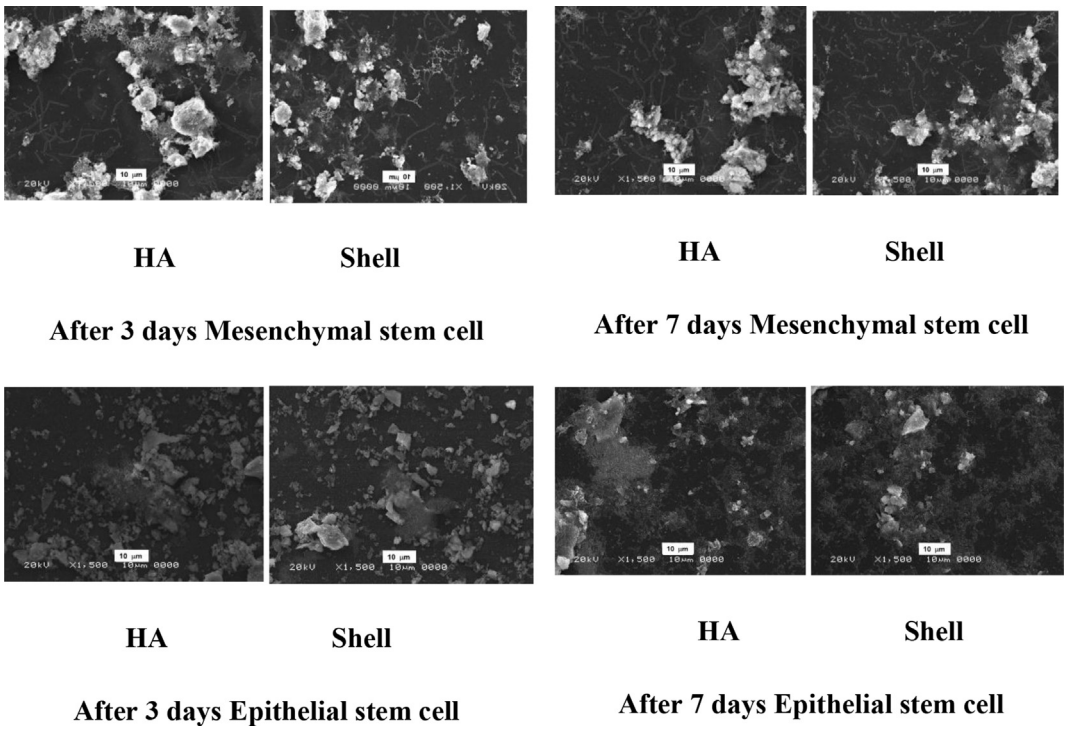

Figure 9. SEM photographs of normal cells (e.g., MSCs and epithelial) after 3 and 7 days of cell culture show the complete association between the cells and material.

HA nanoparticles with COO^- anions and NH_4^+ cations of the BSA protein [39, 41].

The characteristic vibrational groups of BSA adsorbed on HA nanoparticles are shown in Figure 10. The characteristic PO_4^{3-} band appeared in a range from 1,000 to 1,100 cm^{-1}. The bands at 1,636 cm^{-1} and 1,474 cm^{-1} were attributed to the C=O stretching vibration of amide I and bending vibration of N–H of amide II, respectively. After protein adsorption, splitting was detected at 1,049 and 925 cm^{-1}, which could be attributed to the P=O and P–O stretching bands of the PO_4^{3-} group, respectively [42]. It seems that, due to the ion exchange between BSA and HA, there was an increase in the amide I band recorded at 1,636 cm^{-1} and an increase in the amide II band (1, 474 cm^{-1}), which prove the compatibility of the helix structure of BSA [43].

The typical band of the amide group indicated the bonding behavior of BSA and HA nanoparticles. This bonding might be due to electrostatic interactions, which are dominant compared to the van der Waals forces related to the hydrophilic behavior. Hereafter, this distinction supports the hydrophobicity of the protein molecules [44].

4. Conclusions

Hydroxyapatite nanoparticles were synthesized beginning with mussel shells. The samples were characterized by XRD, SEM/EDX, TEM

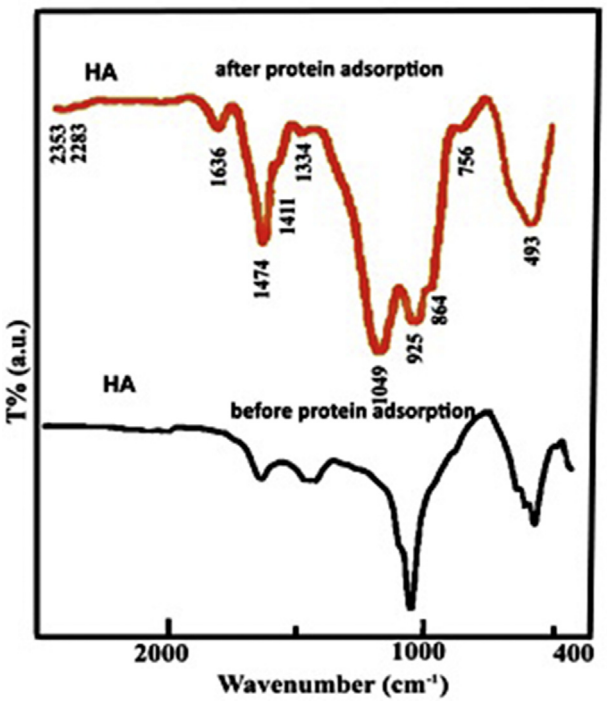

Figure 10. FTIR spectra of HA (calcined at 900°C/2 h) samples before and after protein adsorption.

and FTIR analyses, which demonstrated the presence of hydroxyapatite as clusters at nanoparticle sizes. The tested materials showed weaker cytotoxicity toward all solid tumor cells. HA and mussel shells are safe for human mesenchymal stem cells (h-MSCs) and epithelial cells. We found that additional MSCs and epithelial cells bound more to HA and mussel shells with an immersion time of 7 days compared to an immersion time of 3 days. The protein adsorption results showed that BSA had a strong binding ability to the HA surface. The development of stem cell biology and nanotechnology has improved the characteristics of tissue engineering by increasing the attachment, proliferation and differentiation of stem cells in vitro. Hence, modified nanomaterials need additional in vivo studies to improve organ transplantation.

Declarations

Author contribution statement

Gehan T. El-Bassyouni, Samah S. Eldera, Sayed H. Kenawy, Esmat M.A. Hamzawy: Conceived and designed the experiments; Performed the experiments; Analyzed and interpreted the data; Contributed reagents, materials, analysis tools or data; Wrote the paper.

Funding statement

This research did not receive any specific grant from funding agencies in the public, commercial, or not-for-profit sectors.

Competing interest statement

The authors declare no conflict of interest.

Additional information

No additional information is available for this paper.

References

[1] A.O.J. Fakoya, D.A. Otohinoyi, J. Yusuf, Current trends in biomaterial utilization for cardiopulmonary system regeneration, Stem Cell. Int. (2018) 32. Article ID 3123961.
[2] D. Núñez, E. Elgueta, K. Varaprasad, P. Oyarzún, Hydroxyapatite nanocrystals synthesized from calcium rich bio-wastes, Mater. Lett. 230 (2018) 64–68.
[3] G.T. El-Bassyouni, S.H. Kenawy, R.S. Hassan, M. Mabrouk, E.M.A. Hamzawy, Removal of 137Cs and 152+154Eu using hydroxyapatite prepared from mussel shells, Inter. Ceramic. Rev. 68 (6) (2019) 34–41.
[4] H.H. Beherei, G.T. El-Bassyouni, K.R. Mohamed, Modulation, characterization and bioactivity of new biocomposites based on apatite, Ceram. Int. 34 (2008) 2091–2097.
[5] K. R Mohamed, H.H. Beherei, G.T. El Bassyouni, N. El Mahallawy, Fabrication and mechanical evaluation of hydroxyapatite/oxide nano-composite materials, Mater. Sci. Eng. C 33 (2013) 4126–4132.
[6] T.A. Salah, A.M. Mohammad, M.A. Hassan, B.E. El-Anadouli, Development of nano-hydroxyapatite/chitosan composite for cadmium ions removal in wastewater treatment, J. Taiwan Inst. Chem. Eng. 45 (2014) 1571–1577.
[7] S. Al-Himdani, Z.M. Jessop, A. Al-Sabah, E. Combellack, A. Ibrahim, S.H. Doak, A.M. Hart, C.W. Archer, C.A. Thornton, I.S. Whitaker, Tissue engineered solutions in plastic and reconstructive surgery: principles and practice, Frontiers in Surgery 4 (2017) 1–14.
[8] A.C. Yorukoglu, A.E. Kiter, S. Akkaya, N.L. Satiroglu-Tufan, A.C. Tufan, A concise review on the use of mesenchymal stem cells in cell sheet-based tissue engineering with special emphasis on bone tissue regeneration, Stem Cell. Int. 2017 (2017) 13. Article ID 2374161.
[9] R. Rohban, T.R. Pieber, Mesenchymal stem and progenitor cells in regeneration: tissue specificity and regenerative potential, Stem Cell. Int. 2017 (2017) 16. Article ID 5173732.
[10] M. Ahmadi, E. Seyedjafari, S.J. Zargar, G. Birhanu, A. Zandi-Karimi, B. Beiki, K. Tuzlakoglu, Osteogenic differentiation of mesenchymal stem cells cultured on PLLA scaffold coated with Wharton's Jelly, Experimental Clin. Sci. J. 16 (2017) 785–794.
[11] H. Shi, W. Zong, X. Xu, J. Chen, Improved biphasic calcium phosphate combined with periodontal ligament stem cells may serve as a promising method for periodontal regeneration, Am J Transl Res 10 (12) (2018) 4030–4041. ISSN: 1943-8141/AJTR0076902, PMID: 30662648.
[12] C. Fu, H. Bai, J. Zhu, Z. Niu, Y. Wang, J. Li, X. Yang, Y. Bai, Enhanced cell proliferation and osteogenic differentiation in electrospun PLGA/hydroxyapatite nanofiber scaffolds incorporated with graphene oxide, PloS One 12 (11) (2017), 0188352.
[13] M. Chen, D.Q.S. Le, J. Kjems, C. Bünger, H. Lysdahl, Improvement of distribution and osteogenic differentiation of human mesenchymal stem cells by hyaluronic acid and β-tricalcium phosphate-coated polymeric scaffold in vitro, Bio-Research 4 (1) (2015) 363–373.
[14] H.R.B. Raghavendran, S. Puvaneswary, S. Talebian, M.R. Murali, S.V. Naveen, G. Krishnamurithy, R. McKean, T. Kamarul, A comparative study on in vitro osteogenic priming potential of electron spun scaffold PLLA/HA/col, PLLA/HA, and PLLA/col for tissue engineering application, PloS One 9 (8) (2014), e104389.
[15] X. Sun, W. Su, X. Ma, H. Zhang, Z. Sun, X. Li, Comparison of the osteogenic capability of rat bone mesenchymal stem cells on collagen, collagen/hydroxyapatite, hydroxyapatite and biphasic calcium phosphate, Regen Biomater 5 (2) (2018) 93–103.
[16] C.A. Haynes, W. Norde, Structures and stabilities of adsorbed proteins, J. Colloid Interface Sci. 169 (1995) 313–328.
[17] C.A. van Blitterswijk, J.J. Grote, W. Kuÿpers, H. Blok-van CJG, W.T. Deams, Bioreactions at the tissue/hydroxyapatite interface, Biomaterials 6 (1985) 243–251.
[18] M.I. Jones, H. Barakat, A. Darrell, D.A. Patterson, Production of hydroxyapatite from waste mussel shells, IOP Conf. Ser. Mater. Sci. Eng. 18 (2011) 192002.
[19] M.F. Alif, W. Aprillia, S. Arief, Peat water purification by hydroxyapatite (HAp) synthesized from waste pensi (corbicula moltkiana) shells. International conference on chemistry and material science (IC2MS) 2017, IOP Conf. Ser. Mater. Sci. Eng. 299 (2017), 012002.
[20] M. Sari, Yusuf, Synthesis and characterization of hydroxyapatite based on green mussel shells (perna viridis) with the variation of stirring time using the precipitation method, IOP Conf. Ser. Mater. Sci. Eng. 432 (2018), 012046.
[21] DOXO rubicin, BC Cancer Drug Manual© Developed: September 1994, Revised: 1 May, 2019, pp. 1–12.
[22] R.T. Dorr, D.D. Von-Hoff, in: Drug Monographs. Cancer Chemotherapy Handbook, second ed., Appleton and Lange, Norwalk, Connecticut, 1994, pp. 395–416. ISBN-13: 978- 0838510360. ISBN-10: 0838510361.
[23] N. Koleini, B.E. Nickel, A.L. Edel, R.R. Fandrich, A. Ravandi, E. Kardami, Oxidized phospholipids in Doxorubicin-induced cardiotoxicity, Chem. Biol. Interact. 303 (2019) 35–39.
[24] A.I. Karelin, R.R. Kayumov, Y.A. Dobrovolsky, FTIR spectroscopic study of the interaction between NH_4^+ and DMSO in Nafion, Spectrochim. Acta Mol. Biomol. Spectrosc. 215 (2019) 381–388.
[25] P. Houghton, R. Fang, I. Techatanawat, G. Steventon, P.J. Hylands, C.C. Lee, The sulphorhodamine (SRB) assay and other approaches to testing plant extracts and derived compounds for activities related to reputed anticancer activity, Methods 42 (4) (2007) 377–387.

[26] N.B. Singh, N.P. Singh, Formation of CaO from thermal decomposition of calcium carbonate in the presence of carboxylic acids, J. Therm. Anal. Calorim. 89 (1) (2007) 159–162.
[27] S. Chaturvedi, P.N. Dave, Review on thermal decomposition of ammonium nitrate, J. Energetic Mater. 31 (2013) 1–26.
[28] S. Ramesh, C.Y. Tan, M. Hamdi, I. Sopyan, W.D. Teng, The influence of Ca/P ratio on the properties of hydroxyapatite bioceramics, Proc. of SPIE - The Inter. Society for Optical Eng. 6423 (2007).
[29] K.R. Mohamed, G.T. El-Bassyouni, H.H. Beherei, Chitosan graft copolymers-HA/DBM biocomposites: preparation, characterization, and in vitro evaluation, J. Appl. Polym. Sci. 105 (2007) 2553–2563.
[30] C. Zhao, A. Tan, G. Pastorin, H.K. Ho, Nanomaterial scaffolds for stem cell proliferation and differentiation in tissue engineering, Biotechnol. Adv. 31 (5) (2013) 654–668.
[31] Z. Geng, Q. Yuan, X. Zhuo, Z. Li, Z. Cui, S. Zhu, Y. Liang, Y. Liu, H. Bao, X. Li, Q. Huo, X. Yang, Synthesis, characterization, and biological evaluation of nanostructured hydroxyapatite with different dimensions, Nanomaterials 7 (2017) 38.
[32] R.G. Geesink, Osteoconductive coatings for total joint arthroplasty, Clin. Orthop. Relat. Res. 395 (2002) 53–65.
[33] J. Dumbleton, M.T. Manley, Hydroxyapatite-coated prostheses in total hip and knee arthroplasty, J Bone Joint Surg Am 86 (2004) 2526–2540.
[34] K. Søballe, O.R. Mouzin, L.A. Kidder, S. Overgaard, J.E. Bechtold, The effects of hydroxyapatite coating and bone allograft on fixation of loaded experimental primary and revision implants, Acta Orthop. Scand. 74 (3) (2003) 239–247.
[35] J. Kärrholm, The triplane fracture: four years of follow-up of 21 cases and review of the literature, J. Pediatr. Orthop. Part B 6 (2) (1997) 91–102 (PMID: 9165437).
[36] A. Oryan, A. Kamali, A. Moshiri A, Baghaban M. Eslaminejad, Role of mesenchymal stem cells in bone regenerative medicine: what is the evidence? Cells tissue, Organs 204 (2) (2017) 59–83.
[37] S. Zhang, Hydroxyapatite Coating for Biomedical Application, CRC Press, 2018. Published March 9, 2018 Reference-469 Pages-329 B/W Illustrations ISBN 9781138076167 - CAT# K34179.
[38] P. Schwinté, J.C. Voegel, C. Picart, Y. Haikel, P. Schaaf, B. Szalontai, Stabilizing effects of various polyelectrolyte multilayer films on the structure of adsorbed/embedded fibrinogen Molecules: An ATR-FTIR study, J. Phys. Chem. B 105 (47) (2001) 11906–11916.
[39] S. Dasgupta, A. Bandyopadhyay, S. Bose, Reverse micelle-mediated synthesis of calcium phosphate nanocarriers for controlled release of bovine serum albumin, Acta Biomater. 5 (8) (2009) 3112–3121.
[40] D.T.H. Wassell, R.C. Hall, G. Embery, Adsorption of bovine serum albumin onto hydroxyapatite, Biomaterials 16 (9) (1995) 697–702.
[41] N. Brandes, P.B. Welzel, C. Werner, L.W. Kroh, Adsorption-induced conformational changes of proteins onto ceramic particles: differential scanning calorimetry and FTIR analysis, J. Colloid Interface Sci. 299 (1) (2006) 56–69.
[42] J.L. Arrondo, A. Muga, J. Castrasena, F.M. Goni, Quantitative studies of the structure of proteins in solution by Fourier-transform infrared spectroscopy, Prog. Biophys. Mol. Biol. 59 (1) (1993) 23–56.
[43] S. Dasgupta, S.S. Banerjee, A. Bandyopadhyay, S. Bose, Zn and Mg-doped hydroxyapatite nanoparticles for controlled release of protein, Langmuir 26 (7) (2010) 4958–4964.
[44] B. Basu, S.K. Swain, D. Sarkar, Cryogenically cured hydroxyapatite-gelatin nanobiocomposite for bovine serum albumin protein adsorption and release, RSC Adv. 3 (2013) 14622–14633.